Lipid Specificity of Surfactant Protein B Studied by Time-of-Flight Secondary Ion Mass Spectrometry

D. Breitenstein,* J. J. Batenburg,† B. Hagenhoff,‡ and H.-J. Galla*
*Institute of Biochemistry, Muenster, Germany; †Department of Biochemistry and Cell Biology, Utrecht University, Utrecht, The Netherlands; and ‡Tascon, Muenster, Germany

ABSTRACT One of the key functions of mammalian pulmonary surfactant is the reduction of surface tension to minimal values. To fulfill this function it is expected to become enriched in dipalmitoylphosphatidylcholine either on its way from the alveolar type II pneumocytes to the air/water interface of the lung or within the surface film during compression and expansion of the alveoli during the breathing cycle. One protein that may play a major role in this enrichment process is the surfactant protein B. The aim of this study was to identify the lipidic interaction partner of this protein. Time-of-flight secondary ion mass spectrometry was used to analyze the lateral distribution of the components in two SP-B-containing model systems. Either native or partly isotopically labeled lipids were analyzed. The results of both setups give strong indications that, at least under the specific conditions of the chosen model systems (e.g., concerning pH and lipid composition), the lipid interacting with surfactant protein B is not phosphatidylglycerol as generally accepted, but dipalmitoylphosphatidylcholine instead.

INTRODUCTION

Mammalian pulmonary surfactant is a complex lipid/protein mixture that is secreted by alveolar epithelial cells, and forms what is most likely a multilayer structure at the air/water interface of the lung (1). Because of one of its main functions—the reduction of surface tension at the air/water interface of the lung—this multilayer structure is supposed by most (e.g., (5)), but not all authors (2), to be highly enriched in disaturated phosphatidylcholines like dipalmitoylphosphatidylcholine (DPPC).

One protein that may play a major role in this enrichment process within the hypophase of the alveoli is the surfactant protein B (SP-B). SP-B is a 79-amino-acid-containing, amphipathic homodimer (3). It is secreted by alveolar type II pneumocytes together with the lipid components of the pulmonary surfactant (4). Because of its net-positive charge (5), and based on results of electron spin resonance spectroscopic studies (6), it is expected to interact with the net-negatively charged lipid phosphatidylglycerol (PG). Nevertheless, further experimental data that either support or contradict this hypothesis are rare.

One approach to investigate the properties of surfactant proteins is the use of surfactant model systems (reviewed by Perez-Gil (7)). Instead of analyzing complex lipid/protein mixtures extracted from the lung, the purified protein is added to a well-defined mixture of lipid components. For the investigation of SP-B most commonly a ternary DPPC/PG/SP-B mixture is used, in which the DPPC content is ~70–80 mol % and the content of protein is below 1 mol % (e.g., (12,13,11)) as the ratio of lipid species and the amount of protein within these model systems is in line with the values found in lavaged mammalian surfactant (8–10).

The investigation of such model systems by the Langmuir film balance technique and fluorescence light microscopy led to the information that, on the one hand, the protein is dissolved in the fluid phase of the surface film upon compression of the system at low surface pressures (11). On the other hand, a kink in the pressure-area isotherm indicates the formation of three-dimensional protrusions at high surface pressures. These protrusions are detectable in scanning force micrographs of transferred Langmuir-Blodgett films (12,13). Nevertheless, none of these approaches actually allow us to conclude on the chemical composition of the observed structures.

Recently, time-of-flight secondary ion mass spectrometry (TOF-SIMS) has become a powerful tool to investigate Langmuir-Blodgett films (14–19). In TOF-SIMS the impact of primary ions leads to a desorption of secondary ions that are characteristic of the surface composition in the uppermost monolayer (20). The secondary ions can be detected as a function of mass and spatial point of origin. Thus, a chemical map can be generated showing the lateral distribution of chemical components down to a resolution of 100 nm (21,22).

With TOF-SIMS it was possible to investigate the complex hydrophobic extract of pulmonary surfactant (17) or a more simple surfactant protein-C-containing ternary-surfactant model system (15). The protein distribution within these mixtures was identified. However, when analyzing different phospholipids the resulting mass spectra in the low mass range (fragment ions) are very similar. A differentiation between phospholipid species normally requires the detection of the intact quasi-molecular ions (15). Using standard instrumentation the secondary ion yields of intact species are comparatively low (23). For this reason, a mapping of the lateral lipid distribution becomes difficult. One approach to solve this problem, as introduced in this article, is the use of

Submitted September 3, 2005, and accepted for publication February 17, 2006.

Address reprint requests to H.-J. Galla, Tel.: 0049-251-833-3201; E-mail: gallah@uni-muenster.de.

0006-3495/06/08/1347/10 $2.00 doi: 10.1529/biophysj.105.073247

deuterated lipid components. Assuming the same fragmentation pattern within a TOF-SIMS analysis, deuterated lipids should be easily distinguished from isotopically unlabeled lipids by the different masses of their fragment ions.

In our experimental setup we investigated a DPPC/PG/SP-B (80:20:0.4 mol %) surfactant model system. As PG component we used either the native dipalmitoylphosphatidylglycerol (DPPG) or the fatty acyl chain deuterated d62DPPG. Our aim was to detect the protein and the lipid distribution within Langmuir-Blodgett films that were transferred below and above the surface pressure of protrusion formation. With our approach we tried to visualize a protein-induced demixing process and to identify the lipid interaction partner of the protein.

MATERIALS AND METHODS

Materials

1,2-Dipalmitoyl-*sn*-glycero-3-phosphocholine (DPPC), 1,2-dipalmitoyl-*sn*-glycero-3-[phospho-*rac*-(1-glycerol)] (DPPG), and palmitoyl chain-deuterated DPPG (d62DPPG) were purchased from Avanti Polar Lipids (Alabaster, AL) and used without further purification. The lipid concentration was determined by a phosphorus assay (24). The fluorophore-labeled lipid BODIPY-PC was purchased from Molecular Probes (Eugene, OR).

Chloroform, methanol, and hexane were HPLC grade and purchased from Roth (Karlsruhe, Germany). Water was purified by a multicartridge system (MilliPore, Billerica, MA) and had a resistivity $>17\ M\Omega \times cm$.

Porcine SP-B was purified from bronchoalveolar lavage fluid by the butanol extraction method (25,26). The protein was free of contaminants as could be seen in electrospray mass spectra and SDS-PAGE. SDS-PAGE under reducing conditions showed it to be a homodimer. By Edman-sequencing, the first 10 N-terminal amino acids were found to be identical with the expected sequence of porcine SP-B.

Lipids and proteins were stored in chloroform/methanol (1:1 vol %). No exchange of deuterium atoms was detected by analyzing the molecular ion signal of d62DPPG in TOF-SIMS.

Tempax glass slides, $25 \times 11 \times 1.1$ mm, were purchased from Rettberg (Gottingen, Germany). Gold (purity 99.999 mol %) was generously supplied by Degussa (Hanau, Germany).

Pressure-area isotherms

Pressure-area isotherms were obtained as described by Krol et al. (12): Measurements were performed on a Wilhelmy film balance (Riegler & Kirstein, Mainz, Germany) with an operational area of 144 cm^2 on pure water at a temperature of 20°C. The lipid/protein mixtures were spread with a microsyringe from the chloroform/methanol solution directly onto the subphase. After an equilibration time of 15 min the monolayers were compressed at a rate of 2.9 cm^2/min.

Fluorescence light microscopy

Domain structures of lipid/protein monolayers comprising the model systems and 0.5 mol % 2-(4,4-difluoro-5-methyl-4-bora-3a,4a-diaza-*s*-indacene-3-dodecanoyl)-1-hexadecanoyl-*sn*-glycero-3-phosphatidylcholine (BODIPY-PC) were visualized by means of fluorescence microscopy (Olympus BX-FLA light microscope equipped with an *x,y* stage, Olympus, Hamburg, Germany).

Preparation of gold supports

Preparation of gold supports was done as described by Buordos et al. (15). Glass slides were cleaned by bath sonication at 70°C, alternately in detergent and water, three times in each case. Immediately before evaporation the slides were dried in a nitrogen stream and further treated with argon plasma in a plasma cleaner (PDC 32G-2, Harrick, Ossining, NY) for 3 min. First, 1 nm of chromium was deposited on the surface of the slide, serving as an adhesive layer, onto which 200 nm of gold were sublimed at a rate of 0.01 nm/s. The gold-covered slides were cleaned by rectification for 8 h in a Soxhlet apparatus using *n*-hexane.

Langmuir-Blodgett transfer

Langmuir-Blodgett (LB) transfers were performed as described by Ross et al. (27) using either freshly cleaved mica plates or gold supports. The substrate was vertically dipped into a pure water subphase of a Langmuir trough (operational area 39 cm^2, Riegler & Kirstein) before spreading the surfactant model system onto the water surface. After 30 min the monolayer was compressed to the required surface pressure with a speed of 1.5 cm^2/min. After equilibrating the system for 15 min the film was deposited onto the support at a speed of 0.7 mm^2/min.

Langmuir-Schaefer transfer

The Langmuir-Schaefer (LS) transfers were carried out as described by Tian et al. (28). The surfactant model system was spread onto a pure water surface. After 30 min the monolayer was compressed to the required surface pressure with a speed of 1.5 cm^2/min. After equilibrating the system for 15 min, a gold support was horizontally dipped onto the surface and immediately lifted up again. In contrast to previous experiments performed by our workgroup (29), the support was not dipped into the subphase because of the necessity of a dry preparation for the vacuum conditions of TOF-SIMS.

Scanning force microscopy

Surface images of the LB-films on mica plates were obtained by using a scanning force microscope from Digital Instruments (Nanoscope IIIa Dimension 3000 microscope; Santa Barbara, CA) with silicon NanoProbe tips (TESP, Digital Instruments, Santa Barbara, CA). The ratio of setpoint amplitude to amplitude A_{sp} of vibration was set to 0.4–0.7 (moderate tapping).

Time-of-flight secondary ion mass spectrometry

TOF-SIMS measurements of surface films transferred onto gold supports were performed in triplicate for all conditions shown. All TOF-SIMS measurements were obtained on a TOF-SIMS IV (IONTOF, Muenster, Germany) using Au^+ as primary ion. Spectra were taken in bunched mode (focus: 3–5 μm) with a mass resolution of 5000–10,000. Cycling time of the instrument was set to 200 μs, allowing the acquisition of spectra up to a mass to charge ratio of 1800. (See Supplementary Material.)

Mass-resolved images were taken at nominal mass resolution (burst alignment mode, focus 300 nm). A surface of $(70)^2\ \mu m^2$ was rastered with 128×128 pixels (pixel size: 550 nm). The primary ion dose did not exceed 8×10^{12} ions/cm^2. In line with observations of Biesinger et al. (19), at this primary ion dose no change or inversion of contrast could be detected in any of the measurements performed.

RESULTS

Comparison of the deuterated and undeuterated system

To verify whether the partly deuterated DPPC/d62DPPG/SP-B system behaves similarly to the undeuterated DPPC/DPPG/SP-B system, the phase behavior of both systems was

analyzed by film balance technique, fluorescence light microscopy and scanning force microscopy.

The pressure-area isotherms of the two model systems show a very similar slope (Fig. 1): The compression of the monolayers leads to an progressive increase of surface pressure. At a molecular area of 47 $Å^2$ and a surface pressure of 39 mN/m, a kink is detectable in the slope. At a molecular area of 44 $Å^2$ the surface pressure increases more rapidly again. Expansion curves differ significantly from the ones obtained during compression: On the one hand, at comparable molecular area the surface pressure is lower than at compression of the surface film. On the other hand, only a slight kink is observable during expansion. At a molecular area larger than 70 $Å^2$ the compression and the expansion isotherms are identical. A second compression of the system does not change the slope of the curves significantly, indicating a high reversibility of the system (data not shown).

In the fluorescence light micrographs, both systems showed dark circular domains with a diameter of 3–10 μm (Fig. 2). With increasing surface pressure the size of the dark domains increases slightly. At a surface pressure of 5 mN/m, however, the partly deuterated system shows smaller domains than the undeuterated system.

We transferred partly deuterated DPPC/d62DPPG/SP-B monolayers at a surface pressure of 50 mN/m onto mica supports and analyzed the samples by scanning force microscopy (SFM, Fig. 3). The samples showed circle- or hexagon-shaped flat domains with a diameter of 2–7 μm surrounded by a protrusion-rich network. The protrusion height varied between 4 and 20 nm. The protrusion height was randomly distributed and no stepwise variation of protrusion height could be detected. This is in line with earlier observations for the undeuterated system (12).

TOF-SIMS spectra

We acquired TOF-SIMS spectra of all components and mixtures used, in order to analyze whether the fragmentation

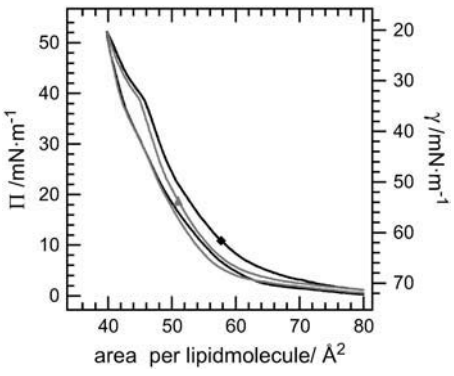

FIGURE 1 Pressure area isotherms of surfactant model systems performed on a Langmuir film balance. Solid diamond, DPPC/DPPG/SP-B (80:20:0.4 mol %); shaded up-triangle, DPPC/d62DPPG/SP-B (80:20:0.4 mol %).

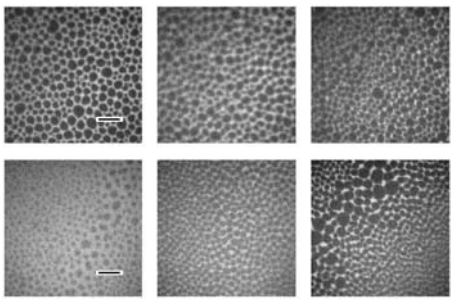

FIGURE 2 Fluorescence light micrographs of surfactant model systems spread on a film balance: (*top*) DPPC/DPPG/SP-B (80:20:0.4 mol %); (*bottom*) DPPC/d62DPPG/SP-B (80:20:0.4 mol %). The pictures are taken at 5 mN/m (*left*), 30 mN/m (*middle*), and 50 mN/m (*right*). The length of the black scalebar is 20 μm.

of DPPC and DPPG with the instrumentation we used is in line with that observed with a slightly different instrumentation (15). In addition, the fragmentation pattern of SP-B was characterized, and the similarity of the fragmentation pattern of deuterated d62DPPG to that of undeuterated DPPG verified.

It was possible to reproduce the spectra observed by Bourdos et al. (15) for DPPC and DPPG, both for positively and for negatively charged secondary ions. In the protein spectra the patterns of the amino acid fragments were detected. The d62DPPG fragmented like DPPG: the fragment ions of the acyl chains showed the expected increased mass/charge ratio.

The fragmentation pattern of DPPC and DPPG turned out to be very similar. A differentiation, however, is

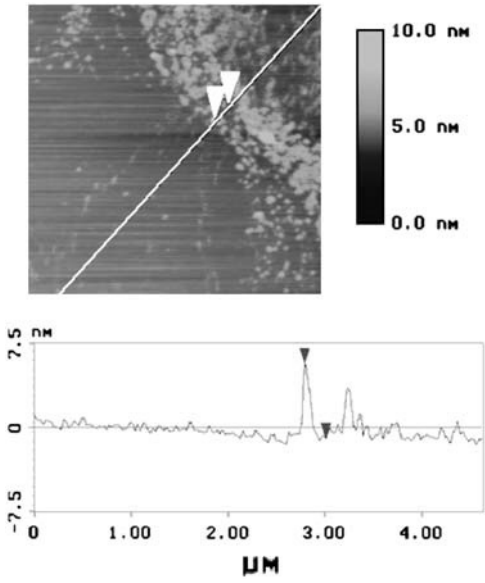

FIGURE 3 Scanning force micrograph of a Langmuir Blodgett transferred (Π = 50 mN/m), partly deuterated surfactant model system DPPC/d62DPPG/SP-B (80:20:0.4 mol %).

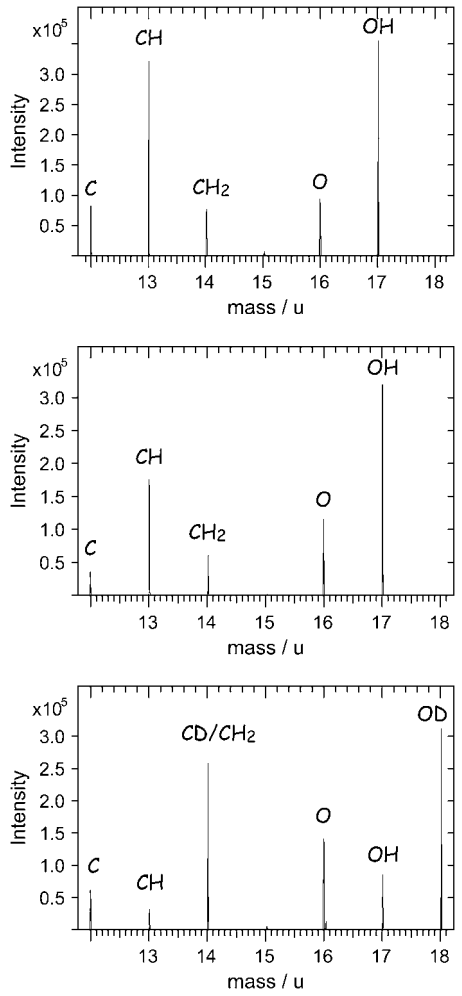

FIGURE 4 Part of TOF-SIMS spectra of DPPC (*top*), DPPG (*middle*), and d62DPPG (*bottom*). Although the spectra of DPPC and DPPG are indistinguishable in this part of the spectra, the analysis of d62DPPG leads to a different fragmentation pattern.

possible for the deuterated component in the low mass range (Fig. 4).

The d62DPPG spectrum shows a significantly different fragmentation pattern: e.g., a fragment ion at a mass/charge ratio of 18 (OD^-) can be detected. The intensity of the fragment ion with the mass/charge ratio of 17 is comparably low, as OH^- ions are formed in lower amount for the partly deuterated molecule. These effects can be observed over the complete mass range in the TOF-SIMS spectra, leading to the following information: while in the undeuterated DPPC/DPPG/SP-B system only the negatively charged quasi-molecular ion of DPPG can be attributed to this lipid, in a spectrum of the DPPC/d62DPPG/SP-B system numerous fragment ions can be attributed to d62DPPG. Thus, numerous mass-resolved images of the DPPC/d62DPPG/SP-B system can be attributed to the phosphatidylglycerol-component allowing us to evaluate mass-resolved images with high ion intensities.

TOF-SIMS mass-resolved images

TOF-SIMS mass-resolved images were obtained for the two mixtures DPPC/DPPG/SP-B and DPPC/d62DPPG/SP-B at surface pressures below (30 mN/m) and above (50 mN/m) the protrusion formation of the monolayer.

Mass-resolved images of the undeuterated system

TOF-SIMS mass-resolved images can be generated both for positively (Fig. 5) and for negatively (Fig. 6) charged secondary ions. Numerous ion images show a networklike structure surrounding round domains both at a surface pressure of 30 mN/m and at 50 mN/m. In these images either the networklike structures or the domainlike structures can be detected with highest yields. (Note that the yield is equal to the number of secondary ions compared to the number of primary ions.) The diameter of the domainlike structures is 2–20 μm.

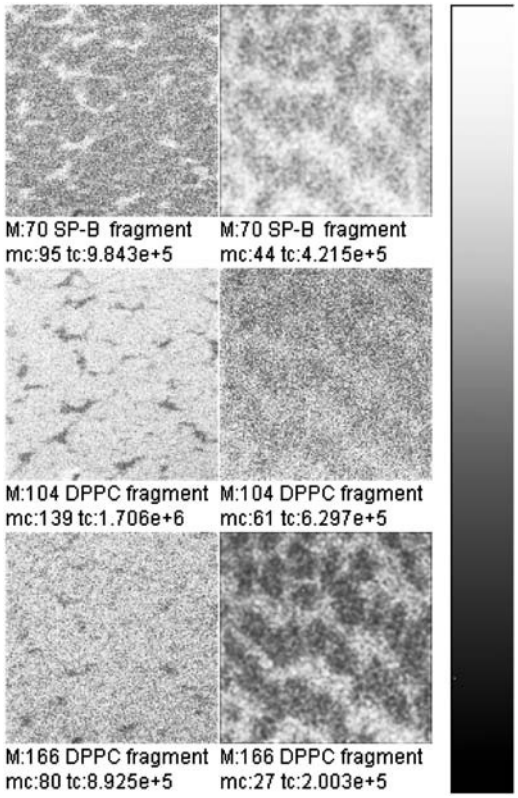

FIGURE 5 TOF-SIMS mass-resolved images of positively charged secondary ions of the system DPPC/DPPG/SP-B (80:20:0.4 mol %) at 30 mN/m (*left*) and at 50 mN/m (*right*). The fragment ions with the mass/charge ratio of 70 ($C_4H_8N^+$, SP-B-specific), 104 ($C_5H_{11}NO^+$, DPPC-specific), and 166 ($C_5H_{13}PNO_3^+$, DPPC-specific) are shown. Ion intensities are represented by a grayscale (see *shaded bar*), with dark colors representing low intensities and bright colors representing high intensities. For each image, white is set to the intensity in the brightest pixel (normalization). This intensity is referenced after ''mc.'' The legend ''tc'' refers to the total number of detected secondary ions in the respective image.

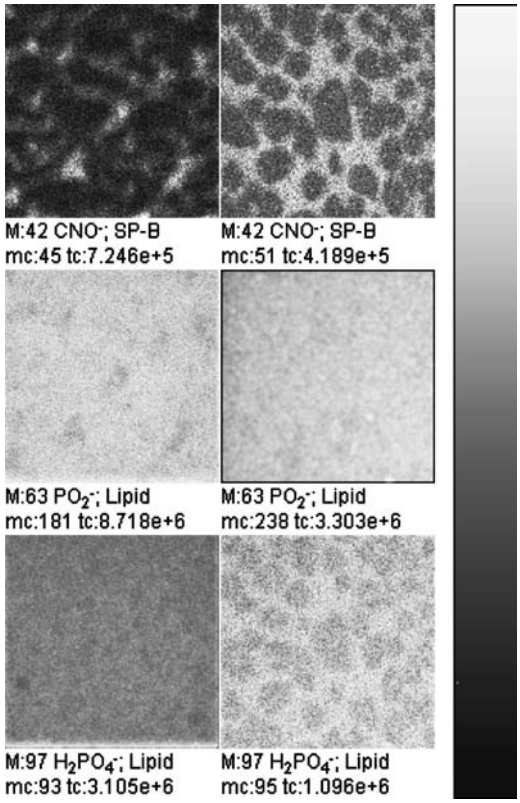

FIGURE 6 TOF-SIMS mass-resolved images of negatively charged secondary ions of the system DPPC/DPPG/SP-B (80:20:0.4 mol %) at 30 mN/m (*left*) and at 50 mN/m (*right*). The fragment ions with the mass/charge ratio of 42 (CNO^-, protein-specific), 63 (PO_2^-, lipid-specific), and 97 ($H_2PO_4^-$, lipid-specific) are shown. Ion intensities are represented by a grayscale (see *shaded bar*), with dark colors representing low intensities and bright colors representing high intensities. For each image, white is set to the intensity in the brightest pixel (normalization). This intensity is referenced after ''mc.'' The legend ''tc'' refers to the total number of detected secondary ions in the respective image.

In Fig. 5, the fragment ions with the mass/charge ratio of 70, 104, and 166 are shown. These fragment ions can be attributed to the fragments $C_4H_8N^+$, which is a typical protein fragment of the amino-acid proline, and to $C_5H_{14}NO^+$ and $C_5H_{13}PNO_3^+$, which are typical PC headgroup fragments. Beside these ions, numerous other ions can either be attributed to the protein or to DPPC (Table 1). All protein-specific fragments show highest ion yields in networklike structures both at 30 mN/m and at 50 mN/m. All DPPC-specific ions are detectable with highest ion yields in domain structures at 30 mN/m and with highest ion yields in the networklike structures at 50 mN/m. As described in the Introduction and for the results of the TOF-SIMS mass spectra, DPPG-specific secondary fragment ions are not detectable under these conditions.

In the negative polarity the protein-specific ions (e.g., $m/z = 42$, CNO^-) show the same distribution as the positively charged protein ions (Fig. 6). In this polarity no fragment ions are detectable that can be attributed on theoretical

TABLE 1 Areas of highest ion yields for a selection of positively charged secondary ions in the DPPC/DPPG/SP-B model system

			Surface pressure	
m/z	Empirical formula	Origin	30 mN/m	50 mN/m
58	$C_5H_8N^+$	DPPC	+	–
59	$C_5H_9N^+$	DPPC	+	–
86	$C_5H_{12}N^+$	DPPC	+	–
102	$C_5H_{12}NO^+$	DPPC	+	–
184	$C_5H_{13}PNO_4^+$	DPPC	+	–
28	CH_2N^+	SP-B	–	–
30	CH_4N^+	SP-B	–	–
44	$C_2H_6N^+$	SP-B	–	–
70	$C_4H_8N^+$	SP-B	–	–
120	$C_8H_{10}N^+$	SP-B	–	–

Symbol key: + Indicates highest ion yields within the domains; – indicates highest ion yields within the networklike structure.

grounds to one lipid exclusively. However, interestingly, two of the phosphate-containing ions derived from both lipids show a diverging behavior: while PO_2^- ($m/z = 63$) is detectable with highest ion yields in the domains at both pressures analyzed, and thus behaves like the d62DPPG ions in the partly deuterated system (see below), $H_2PO_4^-$ shows the same contrast inversion as the DPPC-derived positively charged ions in this system. This suggests that the PO_2^- ions are derived relatively more from DPPG and the $H_2PO_4^-$ ions from DPPC. This behavior is also observed in the spectra of the pure DPPG and DPPC spectra.

Of course phosphates may originate from phosphate-containing contaminants. Such contaminants were only found in the pure SP-B spectra. No contaminants were detected in the spectra of the pure lipids. As SP-B is present only in minor concentrations we therefore can assume that the intensity contributions to the phosphate signals mainly originate from the lipids. This assumption is confirmed by the fact that no possible phosphate counterions and no phosphate cluster ions were detected in the mass spectra of the undeuterated mixture. Nevertheless, the attribution of the lipid as characteristic for lipids has to be seen as a hypothesis, since the contribution of a unknown contamination cannot be ruled out completely. A clear identification of the phosphate origin might be possible by using lipids with isotopically labeled phosphate groups.

Mass-resolved images of the deuterated system

As can be seen in Table 2, the results observed for the undeuterated system can be reproduced for the deuterated system.

While protein specific ions like $C_4H_8N^+$ show highest ion yields in the networklike structures (Fig. 7), DPPC-specific ions as the $C_5H_{13}PNO_3^+$ cations invert their contrast upon increasing the pressure from 30 mN/m to 50 mN/m, whereby the lateral organization is changed from domain- to networklike structures, respectively.

TABLE 2 Areas of highest ion yields for a selection of positively charged secondary ions in the DPPC/d62DPPG/SP-B model system

			Surface pressure	
m/z	Empirical formula	Origin	30 mN/m	50 mN/m
86	$C_5H_{12}N^+$	DPPC	+	–
102	$C_5H_{12}NO^+$	DPPC	+	–
104	$C_5H_{14}NO^+$	DPPC	+	–
166	$C_5H_{13}PNO_3^+$	DPPC	+	–
34	$C_2D_5^+$	D62DPPG	+	+
46	$C_3D_7^+$	D62DPPG	+	+
50	$C_4D_7^+$	D62DPPG	+	+
62	$C_4D_9^+$	D62DPPG	+	+
28	CH_2N^+	SP-B	–	–
44	$C_2H_6N^+$	SP-B	–	–
70	$C_4H_8N^+$	SP-B	–	–
120	$C_8H_{10}N^+$	SP-B	–	–

Symbol key: + Indicates highest ion yields within the domains; – indicates highest ion yields within the networklike structure.

Interestingly, d62DPPG-specific ions like $C_4D_7^+$ (m/z = 62) are detectable with highest ion yields in those areas that show low yields for protein fragment ions. At both surface pressures analyzed they occupy a domainlike structure. At 30 mN/m, the highest ion yield is found in the center of the domain in a much smaller area than that of DPPC-specific ions. At 50 mN/m, the contrast of d62DPPG-specific ions is opposite to that of the DPPC-specific ions.

Since with Langmuir-Blodgett films only the side of the surface film directed to the air can be investigated and TOF-SIMS is a analytical tool for the uppermost monolayer, we also performed Langmuir-Schaefer transfer. With this experimental setup we wanted to exclude the following explanation for our TOF-SIMS results on Langmuir Blodgett samples: If d62DPPG is selectively excluded into the protrusions of the surface film by the protein and the protrusions are turned toward the subphase, the d62DPPG fragment ions could be covered by a DPPC-rich monolayer and thus, the d62DPPG within this structures might not be detectable by TOF-SIMS.

This possibility can be excluded by Langmuir-Schaefer transfer, which leads to an upside-down preparation in comparison with Langmuir-Blodgett films. As the results of the Langmuir-Schaefer transfers done at 50 mN/m are in line with those of the Langmuir-Blodgett films at the same pressure, we can exclude an artifact of d62DPPG covered by DPPC and protein material.

A three-color overlay allows a correlation analysis of the lateral distribution of three secondary ion species (Fig. 8). Each ion intensity is plotted in a pure color scale (*red*, *green*, *blue*). Areas where more than one species is present appear in the respective mixed color (positive color addition: *red* + *blue*, *magenta*; *red* + *green*, *yellow*; *green* + *blue*, *light blue*; *red* + *green* + *blue*, *white*).

The mass-resolved images of negatively charged ions (Fig. 9) are in line with the results for positively charged ions: The networklike structure of protein-derived ions like

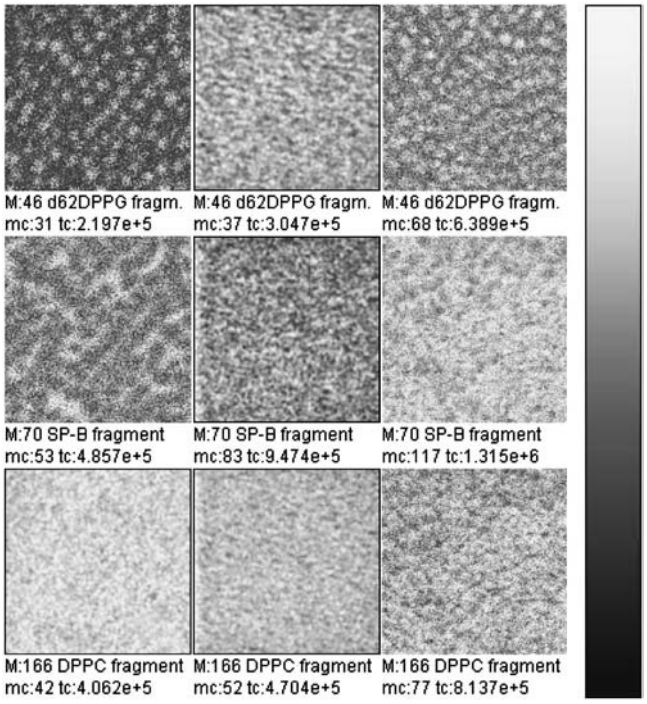

FIGURE 7 TOF-SIMS mass-resolved images of positively charged secondary ions of the system DPPC/d62DPPG/SP-B (80:20:0.4 mol %) after LB-transfer at 30 mN/m (*left*) and at 50 mN/m (*middle*) as well as after LS-transfer at 50 mN/m (*right*). The fragment ions with the mass/charge ratio of 46 ($C_3D_5^+$, d62DPPG-specific), 70 ($C_4H_8N^+$, protein-specific), and 166 ($C_5H_{13}PNO_3^+$, DPPC-specific) are shown. Ion intensities are represented by a grayscale (see *shaded bar*), with dark colors representing low intensities and bright colors representing high intensities. For each image, white is set to the intensity in the brightest pixel (normalization). This intensity is referenced after ''mc.'' The legend ''tc'' refers to the total number of detected secondary ions in the respective image.

CNO^- can be observed at both surface pressures investigated. While d62DPPG-specific secondary ions like D^- show highest ion yield in the domainlike structures at both surface pressures, DPPC-specific ions like the undeuterated palmitic acid anion change their contrast from domainlike to networklike upon surface pressure increase. As can be seen in an overlay (Fig. 10), the DPPC anions require a greater area of the domainlike structure than the d62DPPG specific ions.

DISCUSSION

The purpose of the investigations described in this report was to identify the lateral distribution of components in a pulmonary surfactant model system containing DPPC/DPPG/SP-B by TOF-SIMS. To maximize the information available from TOF-SIMS experiments both the isotopically unlabeled DPPC/DPPG/SP-B (80/20/0.4 mol %) and the partially deuterated DPPC/d62DPPG/SP-B (80/20/0.4 mol %) system were analyzed.

It was expected that the SP-B/DPPG interaction proposed by other authors (e.g., (5,7)) would result in an identical distribution of SP-B- and DPPG-specific secondary ions,

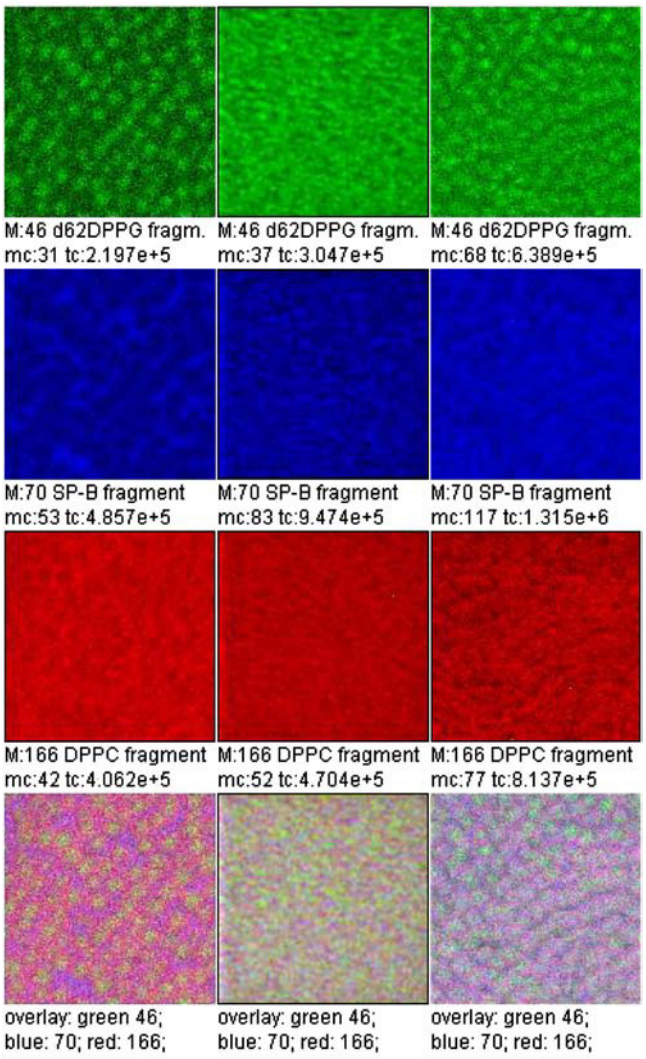

FIGURE 8 Overlay of TOF-SIMS mass-resolved images of positively charged secondary ions of the system DPPC/d62DPPG/SP-B (80:20:0.4 mol %) after LB-transfer at 30 mN/m (*left*) and at 50 mN/m (*middle*) as well as after LS-transfer at 50 mN/m (*right*). The fragment ions with the mass/charge ratio of 46 ($C_3D_5^+$, d62DPPG-specific), 70 ($C_4H_8N^+$, protein-specific), and 166 ($C_5H_{13}PNO_3^+$, DPPC-specific) are shown (rows *1–3*) and used to perform an overlay (row *4*).

whereas the distribution of SP-B- and DPPC-specific secondary ions would differ from each other.

Surprisingly, in our experiments SP-B and d62DPPG do not show highest ion yield in the same areas of the surface film in all TOF-SIMS experiments performed. In contrast to the expected results, DPPC- and SP-B-specific secondary ions are at least partially distributed in the same areas of the surface film. Especially at high surface pressure, DPPC and SP-B are colocalized.

Lateral distribution of protein and lipids

The secondary ions detected by TOF-SIMS are in many cases highly specific for one chemical substance. E.g., the

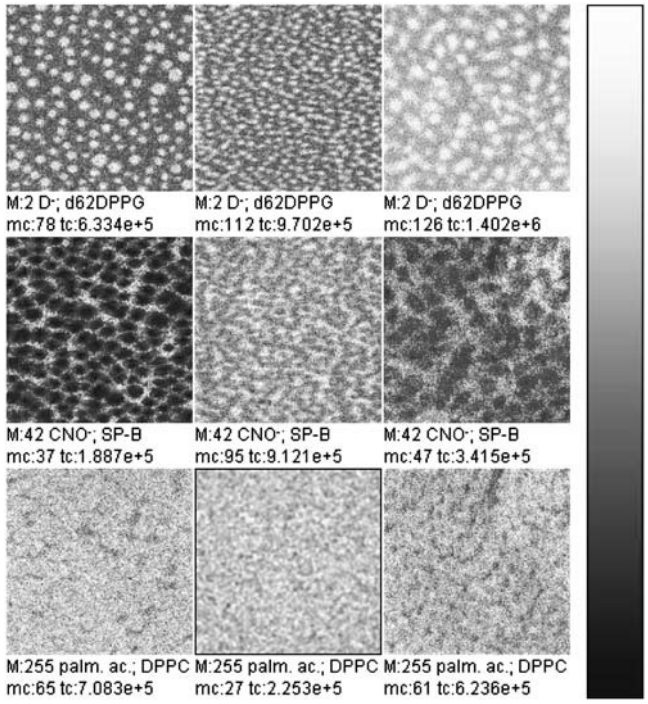

FIGURE 9 TOF-SIMS mass-resolved images of negatively charged secondary ions of the system DPPC/d62DPPG/SP-B (80:20:0.4 mol %) after LB-transfer at 30 mN/m (*left*) and at 50 mN/m (*middle*) as well as after LS-transfer at 50 mN/m (*right*). The fragment ions with the mass/charge ratio of 2 (D^-, d62DPPG-specific), 42 (CNO^-, protein-specific), and 255 (palmitidic acid anion, DPPC-specific) are shown. Ion intensities are represented by a grayscale (see *shaded bar*), with dark colors representing low intensities and bright colors representing high intensities. For each image, white is set to the intensity in the brightest pixel (normalization). This intensity is referenced after ''mc.'' The legend ''tc'' refers to the total number of detected secondary ions in the respective image.

negatively charged secondary ions with $m/z = 26$ and $m/z = 42$ are attributed to the secondary ions CN^- and CNO^-, which are dominantly formed upon protein fragmentation. In both model systems used all protein-specific secondary anions and cations are mainly detected in the networklike structure. The lateral distribution of these fragment ions is not influenced by the surface pressure. This observation can be interpreted as an enrichment in protein in these structures, which is in line with previously reported results (11).

Those fragment ions, which are detected in the domainlike structures with highest secondary ion intensities, are expected to be DPPG or d62DPPG fragments. The PO_2^- secondary ion is not necessarily derived from the (d62) DPPG molecule, but for some of the ions showing the described behavior there is no doubt that they are d62DPPG-specific: E.g., the negatively charged fragment ions with $m/z = 2$ can only be attributed to the deuterium anion and the deuterated palmitic acid anion. Thus, the ion yield of DPPG as well as d62DPPG fragment ions is highest in those areas, where the protein ion yield is lowest.

There are some fragment ions, that can only be observed in lipid systems containing DPPC (e.g., m/z = 166, $m/z = 184$).

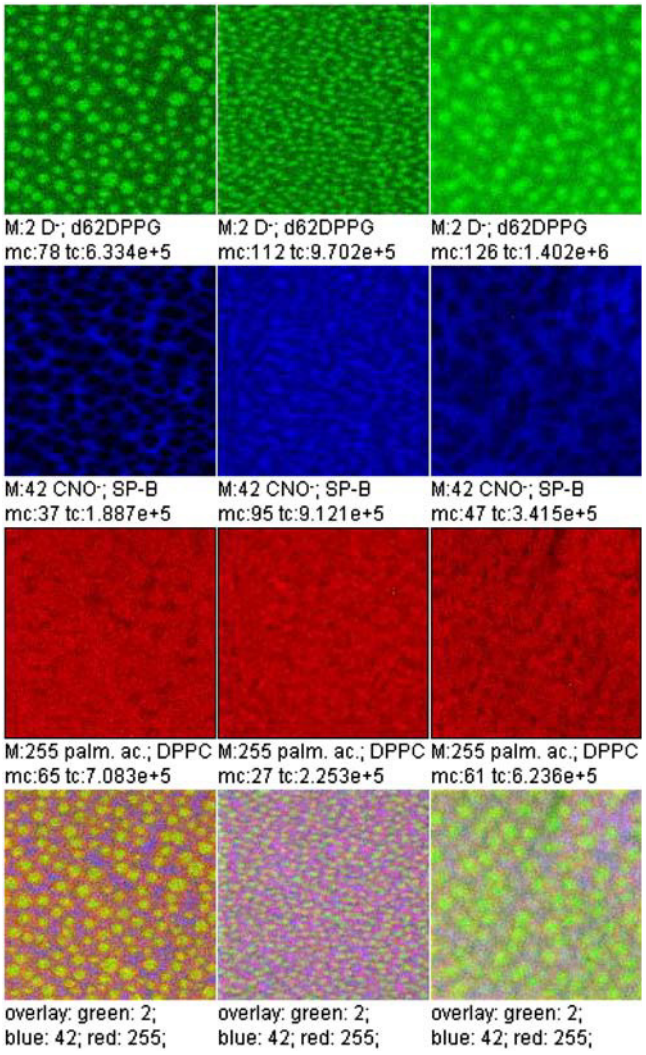

FIGURE 10 Overlay of TOF-SIMS mass-resolved images of negatively charged secondary ions of the system DPPC/d62DPPG/SP-B (80:20:0.4 mol %) after LB-transfer at 30 mN/m (*left*) and at 50 mN/m (*middle*) as well as after LS-transfer at 50 mN/m (*right*). The fragment ions with the mass/charge ratio of 2 (D^-, d62DPPG-specific), 42 (CNO^-, protein-specific), and 255 (palmitidic acid anion, DPPC-specific) are shown (rows *1–3*) and used to perform an overlay (row *4*).

These are headgroup fragments of DPPC such as the positively charged ion with the mass/charge ratio of 184, which is attributed to the $C_5H_{15}PNO_4^+$ ion (16). In our approach, we are also able to detect these DPPC-specific fragments. Their lateral distribution changes upon increasing surface pressure: At 30 mN/m the ion yield of these fragment ions is highest in the domains. The area of highest ion yield of DPPC occupies a larger area part of the domains than the area of d62DPPG-specific fragments. The latter only occupy the center of the domains, while the DPPC-specific ions show high ion yield in a larger domain area. At 50 mN/m, the contrast of the ion yield of the DPPC-specific ions changes. Under these conditions, they are mainly detected in the area of the networklike structures; and the DPPC fragment ions show the same lateral distribution as the SP-B fragments.

Interpretation of the TOF-SIMS results

The lateral distribution of ion yields in TOF-SIMS mass-resolved images of protein- and lipid-containing films is usually interpreted to be identical with the lateral distribution of the material (15–17). This would lead to the following interpretation of our results: At a surface pressure of 50 mN/m, DPPC is mainly distributed in those areas where the protein is distributed. At 30 mN/m, the protein and DPPC are distributed in close contact to each other, but not exactly in the same areas. In contrast to this, d62DPPG is not distributed in the areas of protein distribution either at 30 mN/m or at 50 mN/m.

As the formation of protrusions starts upon compression of a monolayer at a pressure of 39 mN/m (kink in the pressure-area isotherm), the interpretation is in line with the observations, that there is a lipid-poor and protein-rich environment in those areas that condense latest (11). After protrusion formation, i.e., exclusion of protein-rich aggregates, these areas might be overlayed by a DPPC-rich lipid monolayer.

Interpreting our results in this way leads to the following suggestions at least for the specific conditions we have chosen in our experiments:

1. A significant amount of d62DPPG does not interact preferentially with SP-B in the partly deuterated system.
2. SP-B might, at least at high surface pressures, interact with DPPC.
3. As this interpretation would be in contrast to most previous discussions on the lipid specificity of SP-B, alternative explanations for our results need to be discussed:
   - The effect is based on the deuteration of one lipid component;
   - The distribution of the secondary ion intensities is not in line with the distribution of the lipids and the protein, due to matrix effects of TOF-SIMS;
   - The protein interacts with one or a few lipid molecules, opening the possibility for a lipid distribution that is in line with our TOF-SIMS results.

Effect of deuteration of DPPG

The comparison of the two lipid systems DPPC/DPPG/SP-B and DPPC/d62DPPG/SP-B reveals that the deuteration of the DPPG component does not have major effects on the phase and mixing behavior of the monolayers. Although pressure-area isotherms of the two systems are in good agreement to each other, in FLM, SFM, and TOF-SIMS, circularly to hexagonally shaped domains are visible. These domains are generally considered to be liquid condensed phases, which are formed upon compression of the monolayer. The diameter of these domains is 2–20 μm, as can be seen by all

of these techniques. The bright areas in the FLM, the protrusion-rich areas in the SFM, and the domain-surrounding areas in the TOF-SIMS, represent networklike structures that are thought to be enriched in protein (11). For the undeuterated system pressure-area isotherms, FLM and SFM results are in line with previously reported results (13).

The only observable minor difference between both investigated systems is the lower amount and smaller size of condensed areas in the partly deuterated system at low surface pressures, as can be observed in the fluorescence light micrographs. This is indicative of a slightly higher fluidity of the system correlating with a higher transition temperature of the deuterated lipid component (25). This effect has been observed earlier for other partly deuterated lipid mixtures (35).

Nevertheless, in our approach the mixing behavior of the two used systems appears to be similar, as can be seen from the TOF-SIMS results for DPPC- and SP-B-specific ions.

Matrix effects of TOF-SIMS

SIMS is not an inherently quantitative technique. The measured intensity of secondary ions is not only a function of the surface concentration but also an the chemical environment. This behavior is discussed in the literature under the term ''matrix effect'' (18,23,31). Strong matrix effects, e.g., occur for the intensities of metal ions in changing oxygen concentrations or for organic systems when changing the layer thickness from monolayers to multilayers. Sostarecz et al. (18) reported the influence of the chemical environment on the formation of the headgroup fragment at m/z 184 in DPPC. However, since all DPPC-related ions (positive as well as negative ion polarity) in our investigation show the same behavior, we can exclude matric effects by simple proton transfer.

In the context of the discussion here, only the influence of the layer thickness has to be discussed. Generally, when increasing the coverage of a metal substrate with organic material the behavior is as follows (36): In the submonolayer range, the secondary ion yield increases linearly with the coverage (strict quantitative behavior). Highest yields are observed for a coverage in the monolayer range. In the multilayer range, the yield shows itself to be constant independent of surface coverage. Depending on the primary ion used, the yield value in the multilayer range is approximately a factor-of-1.5–5 lower than the yield for the monolayer. Therefore, at the same concentration, in the uppermost monolayer of a sample region with thick organic layers, these appear darker than areas with monolayers on metal substrates.

Concerning the layer thicknesses of the experiments heredescribed, we can state as shown in Table 3.

At 30 mN/m the lateral distribution in the images should therefore represent the surface concentrations, i.e., both DPPG and DPPC are mainly localized in the domain areas, whereas lower intensities are observed for the networklike structures, which are mainly populated by the protein.

TABLE 3 Expected topology of the transferred surface film in the structured observed by TOF-SIMS

	30 mN/m	50 mN/m
Domains	Monolayer	Monolayer
Networklike structure	Monolayer	Nonmonolayer

At 50 mN/m the highest intensities for DPPC are found in the networklike structures together with the protein. Because these structures consist of nonmonolayer areas where the secondary ion yields are generally smaller than in monolayer regions, it can be concluded that, for the investigated system at this surface pressure, DPPC is mainly populating the networklike protein-rich regions. The highest intensities for DPPG are found in the domains at this surface pressure. In the network regions, the intensity of DPPG is smaller, although higher than at 30 mN/m. Because of the above described matrix effect, it is not possible to finally decide whether the surface concentration of DPPG is higher in the domains compared to the networklike structures. Nevertheless, there must be significant amounts of DPPG present in the domains to generate the high signal intensity observed.

Because most investigators expect SP-B to interact with 25–70 lipids (6,32,33), and as it has been shown by theoretical calculations, based on pressure-area isotherms, that DPPC and DPPG do almost mix ideally (34), these results are in line with TOF-SIMS mass-resolved images of the protein-free DPPC/DPPG and DPPC/d62DPPG systems (unpublished data). We therefore expect the demixing effect to be protein-induced.

CONCLUSIONS

The results shown in this study clearly show a lipid demixing in the chosen model systems. Such a lipid demixing process is necessary for the proposed selective enrichment of DPPC in the surface film of the alveoli.

Surprisingly, the results do not show any indication for a preferential SP-B/PG interaction within these model systems. Moreover, under most conditions studied DPPC and SP-B are colocated within the surface film at a surface pressure of 50 mN/m, suggesting that these two model system components can interact under the specific conditions chosen.

As these results are not in line with the common interpretations of electron spin resonance spectroscopy (6) and of vesicle adsorption experiments (7), further investigations on the lipid specificity of the protein with different techniques will be necessary to allow a final conclusion on the lipid specificity of the protein. Moreover, TOF-SIMS results on further model systems under various conditions have to be obtained to allow a generalization of the interpretation offered in this article.

SUPPLEMENTARY MATERIAL

An online supplement to this article can be found by visiting BJ Online at http://www.biophysics.org.

The authors thank Heinrich Luftmann (Institute of Organic Chemistry, University Muenster) for ESI-MS measurements on the protein as well as Michaela Meyer and Reinhard Kersting for critically reading the manuscript.

This work was supported by funds of the Deutsche Forschungsgemeinschaft Sonderforschungsbereich grant No. 424.

REFERENCES

1. Schuerch, S., H. Bachofen, and F. Possmayer. 2001. Surface activity in situ, in vivo, and in the captive bubble surfactometer. *Comp. Biochem. Physiol. A Mol. Integr. Physiol.* 129:195–207.
2. Crane, J. M., and S. B. Hall. 2001. Rapid compression transforms interfacial monolayers of pulmonary surfactant. *Biophys. J.* 80:1863–1872.
3. Curstedt, T., J. Johansson, J. Barros-Soderling, B. Robertson, G. Nilsson, M. Westberg, and H. Jornvall. 1988. Low-molecular-mass surfactant protein type 1. The primary structure of a hydrophobic 8-kDa polypeptide with eight half-cysteine residues. *Eur. J. Biochem.* 172:521–525.
4. Weaver, T. E., C. L. Na, and M. Stahlman. 2002. Biogenesis of lamellar bodies, lysosome-related organelles involved in storage and secretion of pulmonary surfactant. *Semin. Cell Dev. Biol.* 13: 263–270.
5. Hawgood, S., M. Derrick, and F. Poulain. 1998. Structure and properties of surfactant protein B. *Biochim. Biophys. Acta.* 1408:150–160.
6. Perez-Gil, J., C. Casals, and D. Marsh. 1995. Interactions of hydrophobic lung surfactant proteins SP-B and SP-C with dipalmitoylphosphatidylcholine and dipalmitoylphosphatidylglycerol bilayers studied by electron spin resonance spectroscopy. *Biochemistry.* 34: 3964–3971.
7. Perez-Gil, J. 2001. Lipid-protein interactions of hydrophobic proteins SP-B and SP-C in lung surfactant assembly and dynamics. *Pediatr. Pathol. Mol. Med.* 20:445–469.
8. Perez-Gil, J., and M. W. Keough. 1998. Interfacial properties of surfactant proteins. *Biochim. Biophys. Acta.* 1408:203–217.
9. Weaver, T. E., and J. J. Conkright. 2001. Functions of surfactant proteins B and C. *Annu. Rev. Physiol.* 63:555–578.
10. Veldhuizen, R., K. Nag, S. Orgeig, and F. Possmayer. 1998. The role of lipids in pulmonary surfactant. *Biochim. Biophys. Acta.* 1408:90–108.
11. Nag, K., S. G. Taneva, J. Perez-Gil, A. Cruz, and K. M. Keough. 1997. Combinations of fluorescently labeled pulmonary surfactant proteins SP-B and SP-C in phospholipid films. *Biophys. J.* 72:2638–2650.
12. Krol, S., M. Ross, M. Sieber, S. Künneke, H.-J. Galla, and A. Janshoff. 2000. Formation of three-dimensional protein-lipid aggregates in monolayer films induced by surfactant protein B. *Biophys. J.* 79: 904–918.
13. Diemel, R. V., M. M. E. Snel, A. J. Waring, F. J. Walther, L. M. G. van Golde, G. Putz, H. P. Haagsman, and J. J. Batenburg. 2002. Multilayer formation upon compression of surfactant monolayers depends on protein concentration as well as lipid composition. An atomic force microscopy study. *J. Biol. Chem.* 277:21179–21188.
14. Leufgen, K. M., H. Rulle, A. Benninghoven, M. Sieber, and H.-J. Galla. 1996. Imaging time-of-flight secondary ion mass spectrometry allows visualization and analysis of coexisting phases in Langmuir-Blodgett films. *Langmuir.* 12:1708–1711.
15. Bourdos, N., F. Kollmer, A. Benninghoven, M. Ross, M. Sieber, and H.-J. Galla. 2000. Analysis of lung surfactant model systems with time-of-flight secondary ion mass spectrometry. *Biophys. J.* 79:357–369.
16. Bourdos, N., F. Kollmer, A. Benninghoven, M. Sieber, and H.-J. Galla. 2000. Imaging of domain structures in a one-component lipid monolayer by time-of-flight secondary ion mass spectrometry. *Langmuir.* 16: 1481–1484.
17. Harbottle, R. R., K. Nag, N. S. McIntyre, F. Possmayer, and N. O. Petersen. 2003. Molecular organization revealed by time-of-flight secondary ion mass spectrometry of a clinically used extracted pulmonary surfactant. *Langmuir.* 19:3698–3704.
18. Sostarecz, A. G., D. M. Cannon, C. M. McQuaw, S. Sun, A. G. Ewing, and N. Winograd. 2004. Influence of molecular environment on the analysis of phospholipids by time-of-flight secondary ion mass spectrometry. *Langmuir.* 20:4926–4932.
19. Biesinger, M. C., P. Y. Paepegaey, N. S. McIntyre, R. R. Harbottle, and N. O. Petersen. 2002. Principal component analysis of organic monolayers. *Anal. Chem.* 74:5711–5716.
20. Benninghoven, A. 1994. Chemical analysis of inorganic and organic surfaces and thin films using time-of-flight secondary ion mass spectrometry (TOF-SIMS). *Angew. Chem. Int. Ed. Engl.* 33:1023–1043.
21. Hagenhoff, B., and D. Rading. 1998. Ion beam techniques: surface mass spectrometry. *In* Handbook of Surface and Interface Analysis. J. C. Riviere and S. Myhra, editors. M. Dekker, New York. 209–254.
22. Hagenhoff, B. 2000. High resolution surface analysis by TOF-SIMS. *Microchim. Acta.* 132:259–271.
23. Benninghoven, A., F. G. Ruedenauer, and H. W. Werner. 1987. Secondary Ion Mass Spectrometry (SIMS). John Wiley & Sons, New York.
24. Rouser, G., A. N. Siakotos, and S. Fleischer. 1966. Quantitative analysis of phospholipids by thin-layer chromatography and phosphorus analysis of spots. *Lipids.* 1:85–86.
25. Haagsman, H. P., S. Hawgood, T. Sargeant, D. Buckley, R. T. White, K. Drickamer, and B. J. Benson. 1987. The major lung surfactant protein, SP 28–36, is a calcium-dependent, carbohydrate-binding protein. *J. Biol. Chem.* 262:13877–13880.
26. Taneva, S. G., J. Stewart, L. Taylor, and K. M. Keough. 1998. Method of purification affects some interfacial properties of pulmonary surfactant proteins B and C and their mixtures with dipalmitoylphosphatidylcholine. *Biochim. Biophys. Acta.* 1370:138–150.
27. Ross, M., S. Krol, A. Janshoff, and H.-J. Galla. 2002. Kinetics of phospholipid insertion into monolayers containing the lung surfactant proteins SP-B or SP-C. *Eur. Biophys. J.* 31:52–61.
28. Tian, C.-H., G. Zoriniants, R. Gronheid, M. van der Auweraer, and F. C. D. Schryver. 2003. Confocal fluorescence microscopy and AFM of thiacyanine J aggregates in Langmuir-Schaefer monolayers. *Langmuir.* 19:9831–9840.
29. Steinem, C., A. Janshoff, W. P. Ulrich, M. Sieber, and H.-J. Galla. 1996. Impedance analysis of supported lipid bilayer membranes: a scrutiny of different preparation techniques. *Biochim. Biophys. Acta.* 1279:169–180.
30. Guard-Friar, D., C. H. Chen, and A. S. Engle. 1985. Deuterium isotope effect on the stability of molecules: phospholipids. *J. Phys. Chem.* 89: 1810–1813.
31. Hagenhoff. 1997: Quantification in Molecular SIMS. *In* Secondary Ion Mass Spectrometry, Proceedings of the Xth International Conference. A. Benninghoven, B. Hagenhoff, and H. W. Werner. John Wiley & Sons, Chichester, UK. 81–88.
32. Cruz, A., C. Casal, I. Plasencia, D. Marsh, and J. Perez-Gil. 1998. Depth profiles of pulmonary surfactant protein B in phosphatidylcholine bilayers, studied by fluorescence and electron spin resonance spectroscopy. *Biochemistry.* 37:9488–9496.
33. Shiffer, K., S. Hawgood, H. P. Haagsman, B. Benson, J. A. Clements, and J. Goerke. 1993. Lung surfactant proteins, SP-B and SP-C, alter the thermodynamic properties of phospholipid membranes: a differential calorimetry study. *Biochemistry.* 32:590–597.
34. Garidel, P., C. Johann, L. Mennike, and A. Blume. 1997. The mixing behaviour of pseudobinary phosphatidylcholine-phosphatidylglycerol as a function of pH and chain length. *Eur. Biophys. J.* 26:447–459.
35. Baldyga, D., and R. Dluhy. 1998. On the use of deuterated phospholipids for infrared spectroscopic studies of monomolecular films: a thermodynamic analysis of single and binary component phospholipid monolayers. *Chem. Phys. Lipids.* 96:81–97.
36. Schnieders, M., D. Schröder, D. Stapel, H. F. Arlinghaus, and A. Benningoven. 2000, Molecular secondary particle emission from molecular overlayers under SF_5^+ bombardment. *In* Secondary Ion Mass Spectrometry, Proceedings of the XIIth International Conference. Elsevier, Amsterdam, The Netherlands. 263–266.